Optical Properties of Multi-Layered Insulation

Heather M. Rodriguez and Kira J. Abercromby
ESCG/Jacobs Sverdrup
P.O. Box 58447
Houston, TX 77058-8447
Mail code: JE104
E-mail: heather.m.rodriguez@nasa.gov

Mark Mulrooney
ESCG/MEI Technologies
2525 Bay Area Blvd., Suite 300
Houston, Texas 77058

Edwin Barker
NASA Johnson Space Center
2101 NASA Parkway
Houston, TX 77058

ABSTRACT

Multi-layer insulation (MLI) is a material used on rocket bodies and satellites primarily for thermal insulation. MLI is comprised of a variety of materials, layer numbers, and dimensions to satisfy specific design requirements. Typically, it is a sandwich of outward facing copper-colored Kapton layers with inward facing aluminized backing. The inner layers consist of alternating DACRON or Nomex netting and aluminized Mylar. From an orbital mechanics perspective, if this material becomes separated from a spacecraft or rocket body, its orbit will vary greatly in eccentricity due to both its high area-to-mass ratio (A/m) and its susceptibility to solar radiation pressure perturbations. Recently, a debris population was found with high A/m which could be MLI.

Laboratory photometric measurements of one intact piece and three different layers of MLI are presented in an effort to ascertain the characteristics of MLI light curves and aid in identifying the source of the new population. For this paper, the layers used will be consistent with the aforementioned common MLI. Using a robotic arm, the piece was rotated from 0-360 degrees in 10º increments along the object's longest axis. Laboratory photometric data was recorded with a CCD camera and a 300 W Xenon arc light source selected to approximate the solar spectrum. The measurements were taken in white light and using various filters (Johnson Blue (B), Visible (V), and Bessell Red (R)), all taken at an 18 degree (light-object-camera) phase angle selected to closely match typical GEO observations which follow the anti-solar point. As expected, the MLI pieces exhibited characteristics similar to a bimodal magnitude plot of a flat plate, but with photometric features dependent upon the layer composition. To minimize highlight saturation (and consequent loss of intensity information), exposure times were selected empirically based on layer type and filter.

In addition to photometric laboratory measurements, laboratory spectral measurements were acquired for each MLI sample. Spectral data will be combined to match the wavelength region of photometric data to establish a fiduciary reference for the photometric measurements. Not only will this help validate the color photometry, but it will also assist interpretation and analysis of telescopic data. As an example, copper-colored Kapton shows a strong absorption feature near 4800 angstroms. If the observed debris is MLI and the outer layer of copper coloring of Kapton is present, evidence of this material should be seen spectroscopically by the specific absorption feature as well as photometrically (e.g. by using R-B (red-blue) light curves).

Using laboratory photometric and spectroscopic measurements an optical property database is provided for a representative high A/m object. These results should directly aid the accurate interpretation of telescopically

acquired optical orbital debris photometry of both high A/m targets as well as satellites and spacecraft that incorporate MLI.

1. Introduction

A new population of debris in the Geosynchronous (GEO) region has exhibited characteristics of objects with high area-to-mass ratios (A/m). High A/m objects possess variable eccentricity and inclination- a characteristic generally resulting from the pronounced effect of solar radiation pressure. The majority of debris is believed to have an A/m < 1 m^2/kg for fragments between 10 and 20 cm, whereas pieces considered to be a high A/m would include ratios of 1 m^2/kg to 40 m^2/kg [1]. For comparison, a piece of notebook paper has an A/m of 13 m^2/kg using the standard surface area of a rectangle to calculate the area and 6 m^2/kg using the average cross sectional area. The average cross sectional area method is used for all calculations throughout the remainder of this paper [2]. This high A/m debris population is thought to be made of multi-layered insulation (MLI), a common insulation material found on rocket bodies and spacecraft. As a thermal shield, MLI is typically composed of reflective copper-colored Kapton outer layers with aluminized backing. The interior of the MLI consists of alternating layers of DACRON or Nomex netting with aluminized Mylar, where the number of interior layers depends on the purpose and usage of the MLI. To aid telescopic identification of these objects, this study obtained photometric measurements of both intact and separated MLI samples (four pieces total). Specifically, the exterior layer and the inner-most layer of a copper-colored Kapton-type MLI sample with aluminized backing and white DACRON fabric were illuminated individually with a lamp approximating the solar spectrum and imaged with a CCD camera through various colored filters. The samples were also measured with a commercial field spectrometer for comparison with and validation of the photometric data.

This paper will show B-R color index data from all four MLI pieces, mentioned above, at an 18º phase angle. Future studies will acquire B, V, R and B-R, B-V profiles over multiple phase angles for comparison with published telescope data. Fig. 1 shows an example of telescopic data taken with the Johnson B filter (centered at 440 nm and 100 nm wide) and the Johnson R filter (centered at 700 nm and approximately 200 nm wide) for six different GEO satellites at multiple phase angles. A B-R color index of zero indicates the ratio fluxes between the two bandpasses are equivalent. If the B-R color index is greater than or less than zero, this indicates a higher intensity in the red or blue filter, respectively. Using the B-R color index can aid in determination of target material composition [3].

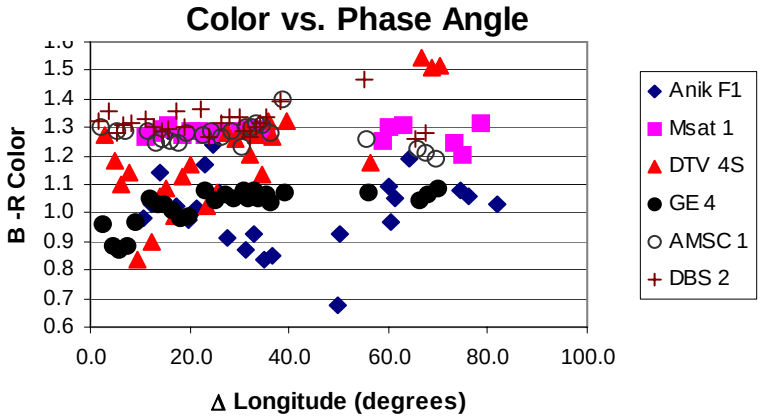

Fig. 1: Example of B-R plot over different phase angles [7].

2. Equipment and Set-Up

2.1 Photometry

The design of the laboratory is analogous to a telescope set-up with a light source, target, and observer. A 300 Watt Xenon arc lamp is used to simulate the solar illumination through the spectral range of 200 to 2500 nm. Since certain layers of the MLI saturate the CCD at the lowest time exposure (0.12 seconds), four neutral density filters are used to reduce the intensity from the source. A simple black board is positioned in front of the light source to keep stray light from scattering into the CCD. The data is acquired through a Santa Barbara Instrument Group (SBIG) ST-8XMEI camera, with a front-side illuminated 1024x1536 pixels, KAF1602E Silicon CCD. A SBIG CFW8A five position filter wheel is attached to the CCD camera, using a standard astronomical suite (Johnson Blue, Visible, and Bessell Red, Infrared). The Blue (B) filter bandpass covers the 350-600 nm range, the Visible (V) filter ranges

from 450-700 nm, the Red (R) filter ranges from 560-1060 nm, and the Infrared (I) filter covers 700-1100 nm. The CCD filter range stops at 1100 nm due to the absorption gap seen in all silicon material, which is used in the ST-8XMEI camera. A telephoto zoom lens (lower-left Fig. 2) is attached to the CCD enabling manual focusing and magnification of targets. The phase angle is that made between the source, target, and CCD camera (top image of Fig. 2) and is set to 18º ± 1º for all the data taken for this paper. This value was chosen to approximate the typical phase angle encountered for telescopic GEO observations near the anti-solar point. A Lynx 6 robotic arm is used to rotate objects through five degrees of freedom (base rotation, shoulder, elbow, wrist, and wrist rotation) in addition to having a functional gripper. As shown in the bottom right image of Fig. 2, the robotic arm is stationed atop a rotary table so that a full 360º rotation may be sampled (wrist rotation is limited to 180º rotation). Details on acquiring the data via the equipment will be addressed in Section 3.

Fig. 2. Digital images taken on laboratory set-up and equipment. Top image: full laboratory set-up. Bottom left image: CCD camera with attached filter wheel and telephoto lens. Bottom Right image: close up on the robotic arm and rotary table.

2.2 Spectroscopy

The spectrometer used is an Analytical Spectral Device (ASD) field spectrometer with a range from 300-2500 nm and a resolving power of approximately 200 (corresponding to a bandwidth of 10 nm at 2000 nm) and 717 channels [4]. The system only needs 210 channels in order to obtain the desired bandwidth, so using 717 channels is over-sampling the data, which results in less degradation of spectral resolution. Measurements are acquired from 350-1100 nm by placing the target under quartz lamp illuminator and orienting the spectrometer's fiber feed (mounted in a pistol grip) approximately perpendicular to the target surface. The data are output to a laptop computer and reduced using in-house developed software to provide the absolute spectral reflectance.

Fig. 3. Set-up for taking spectral measurements: optic pistol grip, quartz lamp, target.

3. Data Acquisition

In an effort to obtain numerous orientations of the object at a set phase angle, the target is rotated within the plane orthogonal to its longest axis. Data is taken every 10º of rotation to sample the full 360º rotation. The 10º step size was determined appropriate after a rigorous comparison between 1, 5, and 10 degree steps showed only a 3% maximum variation in measured intensity between the different sampling intervals. A 10 degree step size also proved sufficient to capture specular reflections that occur mainly when the maximum surface area is visible to the observer.

At each rotation a number of images are taken in each filter to be co-added in MATLAB®. The number of images acquired in each filter is dictated by the need for comparable signal-to-noise (SNR) levels in each. To achieve this, co-adding of frames is employed whereby (following Poisson statistics) SNR improves as roughly the square root of the number of acquired frames. Since the front-side illuminated CCD blue response is quite poor (R-band QE is approximately twice B-band),it was determined empirically that approximately four times as many B-band frames are required as R-band.

Image processing is performed in accordance with standard astronomical techniques [5]:

$$\text{Final Processed Image} = (\text{Raw} - \text{Dark})/\text{Flat}$$

The images are dark subtracted using dark frames acquired at the same exposure as the image exposure to remove CCD thermal noise. Normalized flat fields are then generated and divided into the image. The flat field is used to remove pixel-to-pixel variations (i.e. dust in the optical path system of the CCD or sensitivity variations) and any gradients within the image. Acquiring a good flat field is difficult and if not taken correctly one could mistakenly intensify or reduce points or regions in the final image. The flat fields are taken through each filter at an exposure close to saturation (~46,000 analog-to-digital units for the ST-8XMEI) and co-added similar to the target images. The final co-added flat image for each filter is then normalized by the average of the flat field image.

The targets are held and rotated in front of a black background to simulate a piece of debris in space. The background is removed from the image by cropping an area of the background and finding the average intensity of the background pixels. The background removal process is performed by a series of detailed steps used in digital morphology (uses a 3 x 3 box to fill in gaps within the object's boundary and remove pixels that deviate higher than a set variance from the background's intensity)[6].

To obtain a magnitude, a diffuse sphere (ping-pong ball) painted white was used as a zero magnitude reference for all colors (BVRI). Five images are taken at the same exposure as the respective filter. The images are then averaged within each filter to calculate the relative magnitude of the object. The following formula is used to define the relative absolute magnitude of the target [7]:

$$M(\text{object}) - M(\text{white ball}) = -2.5 * \log_{10} [\text{intensity(object)}/ \text{intensity(white ball)}]$$

Final analysis of the data is completed by creating light curves for each material through every rotation angle for each filter. Following the completion of the data reduction process, the light curves can be compared and examined.

4. Debris Samples

The sample targets are MLI intact, MLI space-facing layer, Dacron interior layer, and MLI spacecraft-facing. The MLI space-facing layer is composed of copper-colored Kapton with an aluminized backing shown in Fig. 4. The surface structure of the space-facing side is a perforated flat surface with a mesh siding used to attach securely the other multiple layers. The interior layers of MLI are made of Dacron or Nomex netting with aluminized Mylar. Only one sample of the interior was used and is shown in Fig. 5. Due to the pliability of the material, all the targets were held taut with pipe cleaners, attached at the edges of the material shown in Fig. 5. The final layer facing the spacecraft is made of copper-colored Kapton with an aluminized backing, reinforced with woven mesh netting, also shown in Fig. 4.

Fig. 4: Top left and right image of Space-facing copper colored Kapton with aluminized backing. Bottom left and right image of spacecraft copper colored Kapton with aluminized backing.

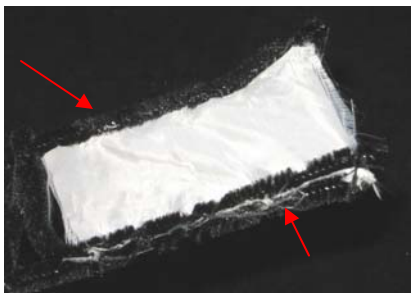

Fig. 5: Image of interior layer of MLI made of Dacron or Nomex Netting. Image enlarged to illustrate pipe cleaners used to hold all pieces taut.

The A/m is calculated using 1/4 of the total surface area for simple convex targets, such as the targets used in this paper. For future targets with complex bodies, one would "determine the view, V, that yields the maximum cross-sectional area and denote the cross-sectional area as Amax. Let A1 and A2 be the cross-sectional areas for the two viewing directions orthogonal to V. Then define the average cross-sectional area as $(A_{max} + A_1 + A_2)/2$." [8]. The A/m ratios for the targets are (from smallest A/m to largest): 2.10 m^2/kg for the intact MLI piece, 4.15 m^2/kg for the spacecraft–facing MLI layer, 5.43 m^2/kg for the space-facing MLI layer, and 10.86 m^2/kg for the MLI sample interior layer. All of these objects are considered to be high A/m.

5. Lightcurve Analysis

Four objects were analyzed in this study and rotated 360° in 10° steps. At each step a full filter suite (BVRI) was used. Due to the nature of these pieces (high A/m), the pipe cleaners used to hold the edges of the pieces rigid for data analysis (see Fig. 5) and the robotic arm grippers are cropped out of the image as much as possible so that the intensity of the material is recorded. If the pipe cleaner is not completely removed from the image during the cropping process, the background removal process usually removes their contribution to the intensity.

Fig. 6 shows intensity scaled by the number of pixels for the four pieces over a 360 degree rotation. Scaling the intensity to the number of pixels shows the true intensity without any system bias (i.e. the background intensity in the blue filter is equivalent to the shadowed areas of the pieces, leading to false intensity dropouts rather than the true intensity based upon the exposed area). This intensity was also scaled by the intensity of the zero reference ball in each filter so that the intensity was not weighted by the sensitivity of the equipment (CCD is red sensitive). The intact piece (top-left of Fig. 6) shows a relatively smooth curve with specular reflections where the maximum surface area is towards the CCD, i.e. between 45 - 90 degrees and 225 - 270 degrees. The object was rotated with the spacecraft-facing side to the CCD and then the final 180 degrees showing the space-facing side to the CCD. Specular reflections were seen on both sides of the MLI material at the maximum exposed area, although the space-facing side had a higher intensity peak, due to the surface structure of the material.

The spacecraft-facing material (top-right Fig. 6) and space-facing MLI (bottom-left Fig. 6) were both rotated so the aluminized side of the material was visible between 0-180 degree rotation and the copper colored Kapton between 180-360 degrees. The intensity in the red wavelengths dominate across the majority of the rotations, which is speculated to be a result of the signal in the red filter far outweighs that of the blue filter. Even with the low signal in the shorter wavelengths, the intensity in the blue filter does show small features (peaks) in the aluminized side of the materials compared to the copper-colored Kapton sides. Both targets were held with more curvature that the other materials, due to the nature of the material, giving rise to the complex structure in the intensity plot in all filters across the entire rotation.

If the spacecraft-facing material and the space-facing material were held with the same rigidity as the intact piece and the contour of these pieces were made to replicate that of the intact, one should expect to see replicated results for the same materials. Therefore the copper-colored spacecraft-facing piece (180-360

degrees) should replicate the intact piece (0-180 degrees) and the copper-colored space-facing piece should mimic the intact piece from 180-360 degrees.

The final plot, bottom-right in Fig. 6, shows the scaled intensity of an interior layer from a MLI piece, white fabric. As expected, the plot does follow smooth shape across all rotations as would be seen by a flat plate rotated across the same rotation angles, where the maximum areas are exposed between 45°-90° and 225°-315°. As with the spectral results, the white fabric photometric results show a higher intensity in the shorter wavelengths than in any other filter.

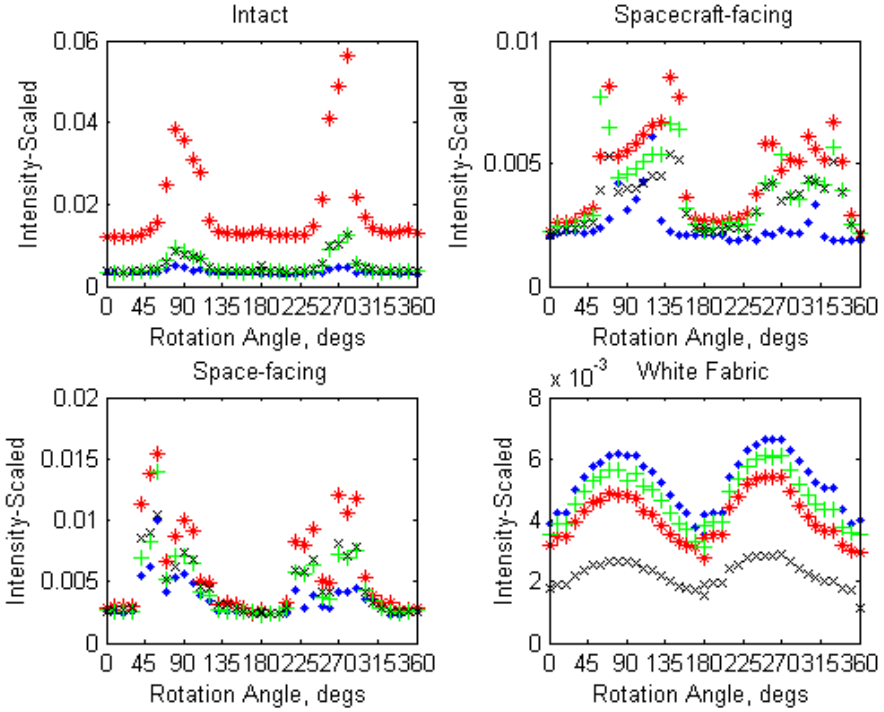

Fig. 6: Intensity scaled by number of pixels of all pieces in all filters. Red '*'=Red filter, Black 'x' = Infrared filter, Green '+' = Visible Filter, and Blue '.'= blue filter.
Note: Aluminized side is exposed from 0-180° and the copper colored Kapton is exposed between 180-360° on the space-facing and spacecraft-facing pieces.

Fig. 7 shows the materials described above, but in a relative magnitude plot over 360 degree rotations. The B-R color index is defined as follows:

$$B - R = -2.5 * \log 10\left(Int_B / Int_R \right),$$

where Int_B and Int_R define the total flux of the object through each respective filter. If a B-R value of zero was obtained, this indicated the intensity in the blue and red filter are equivalent. The positive numbers are indicative of higher intensities in the longer wavelengths (red), where negative numbers signify higher intensities in shorter wavelengths (blue). The intact piece shows that the magnitude in the red filter was brighter, as to be expected with Kapton material from the spectroscopic data. As revealed by the spectroscopic data, Kapton material has higher reflectance in the red and infrared than in the blue or green wavelengths. Since the intact piece has identical material on both sides, the magnitude plot is relatively flat with peaks at the specular points of reflection. The spacecraft-facing and space-facing materials indicate that even with the aluminized side facing the CCD between 0°-180°, there is still not enough signal in the shorter wavelengths to overcome the strong signal in the longer wavelengths. The last plot in Fig. 7, bottom right, shows a flat B-R color index, indicating the intensity is constant and no specular reflections are present. A constant B-R Color index value of approximately -0.1, indicated that the white fabric does in fact have higher signal in the blue filter. This piece makes material identification a struggle since the

difference in B-R and B-V would expectedly all be relatively the same, likewise with the laboratory spectra on this piece.

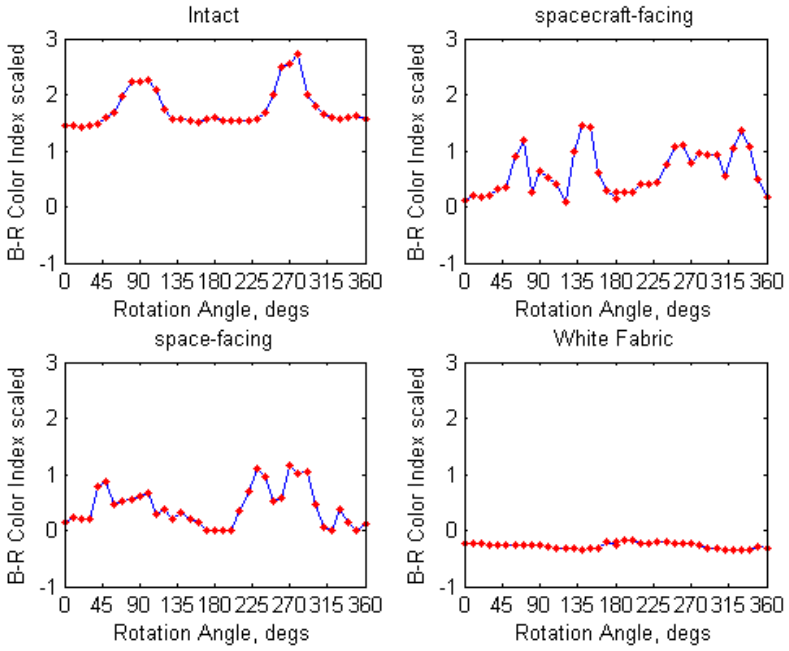

Fig. 7: B-R Color Index scaled by number of pixels of all pieces over all rotations
Note: Aluminized side is exposed from 0-180 degrees and the copper-colored Kapton is exposed between 180-360 on the space-facing and spacecraft-facing pieces.

The values obtained from the B-R plots can be used for comparison for different targets at different phase angles. The data collected for this paper encompasses only one phase angle, but progress continues to extract data analogous to published telescopic data as shown in Fig. 1.

6. Spectral Measurements

As part of the validation process, the laboratory produced spectral data was used as a fiduciary reference and compared to the photometric results in an effort to remove any equipment biases. The methodology for calculating the total system response will be discussed in Section 7.

Spectral reflectance measurements possess much higher wavelength resolution than photometric measurements. For example, when comparing the photometric data already presented there is one value for the V filter whereas spectral measurements contain 250 measurements over the same bandpass. Spectral data was acquired using the identical pieces described earlier. Unlike the photometric samples however, this spectral data will only show a diffuse reflectance and will show no specular component.

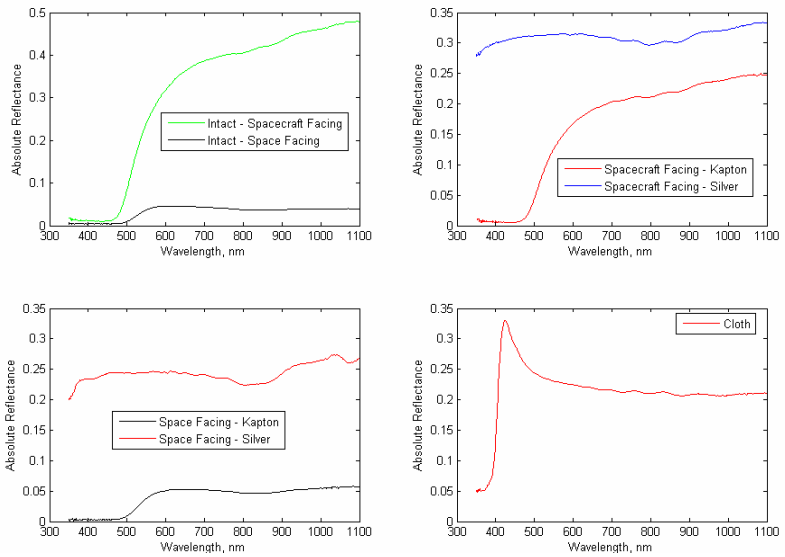

Fig. 8: Laboratory Spectra on all MLI pieces.

In Fig. 8, the data is presented over all wavelengths collected, 350 – 1100 nm. The upper left image shows the intact piece of MLI, both the space-facing and spacecraft-facing directions. The spacecraft-facing side has more stitching on it, allowing for fewer contours, so that more of the reflected light is returned in the direction of the probe. In addition, there is a slight difference in the surface properties between the spacecraft-facing and space-facing materials (e.g. there are more absorption features in the infrared in the spacecraft-facing materials).

The strong absorption due to the copper coloring of MLI starting at 480 nm (4800 angstroms), results in a distinct difference between the B and R response for the spacecraft-facing and space-facing Kapton side versus the aluminized side. It will be more difficult to distinguish the two aluminized (silver colored) materials from the cloth since materials have relatively constant reflectance through the visible regime and therefore the values of B, V, and R should be similar in intensity. If the I band is incorporated, the cloth and silver colored material can be distinguished by using the aluminum feature near 840 nm (8400 angstroms).

7. Total Signal

To properly calibrate the photometric data so that it may be used to interpret telescopic observations, it is necessary to determine the total system throughput for a given source, target, filter and detector combination. In this way the intrinsic response of the target can be ascertained (and this can be further compared with the aforementioned spectroscopic measurements). Once the intrinsic response of the target is known it can be matched to any instrument (e.g. telescope) so that observational results can be properly interpreted (e.g. revealing the relative contributions of various target materials to the observed response).
To obtain the system throughput it is necessary to integrate all the functions acting on the system over a specified range as seen in the following equation [9,10]. The source flux ($F_{SOURCE}(\lambda)$) is defined as the response of the light source over all wavelengths. The light source, 300 Watt Xenon arc lamp, closely matches the UV-VIS solar spectrum, radiating 5500-6000 K, where the Xenon lines dominate between 750-1000 nm. The transmittance through each filter is define by ($T_{FILT}(\lambda)$). The reflectance of the material through the specified wavelength is given by ($R_{TARGET}(\lambda)$) and the CCD Quantum Efficiency is ($QE(\lambda)$).

$$S = \int_{\min range}^{\max range} F_{SOURCE}(\lambda) \cdot T_{FILT}(\lambda) \cdot R_{TARGET}(\lambda) \cdot QE(\lambda) d\lambda$$

Fig. 9 and Fig. 10 show the total signal (S) flux computed for the spacecraft-facing Kapton piece of MLI (copper colored Kapton with mesh surface) in the V filter, ranging from 450-700 nm. Using a least squares fit, the curve function describing the quantum efficiency of the CCD, target's spectra in the specific bandpass, V filter response and the irradiance of the light source are multiplied together to yield one final plot: the total response of the material through the optical system, shown in Fig. 10. For this specific

example a sum of sine function, 5th order sine function, Gaussian function and exponential function were used to fit the following plots (QE, spectra, V filter, and Source Spectrum) respectively with 95% confidence bounds.

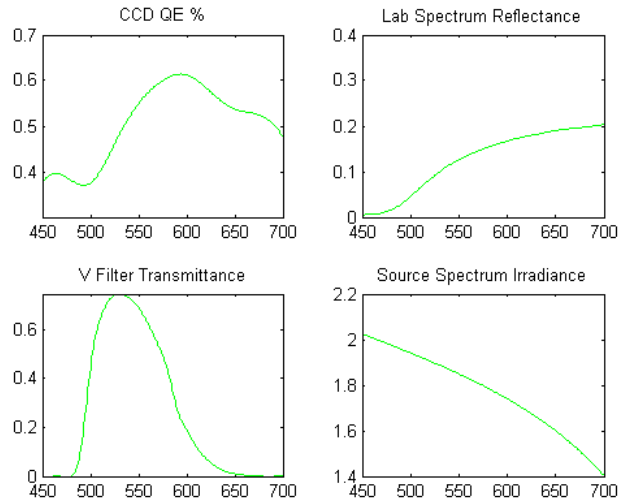

Fig. 9: Specific Curve fits to data for CCD QE, Lab Spectrum for the Spacecraft Kapton, V filter and the light source spectrum over the visible wavelengths (450:700 nm).

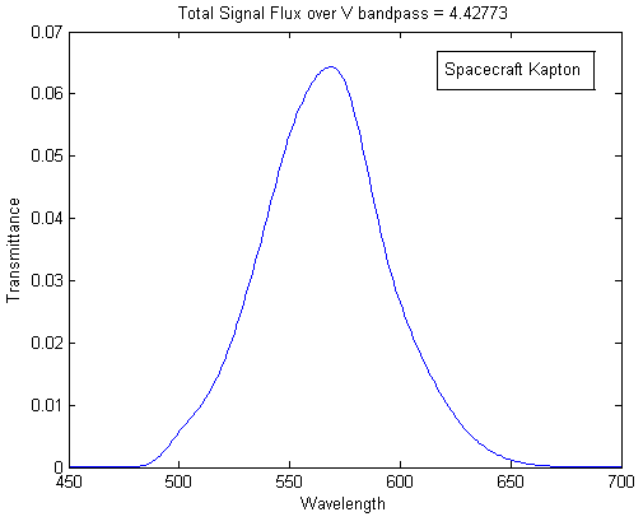

Fig. 10: Plot evaluation of all source functions integrated over the V bandpass for the spacecraft Kapton. Plot shows a 6.5 % transmittance without equipment bias.

Using the integrated value for the filter will allow for one to compare the photometric data to the spectra data through filter comparisons, B-R and others. Seen in Fig. 10, the integrated value for the spacecraft-facing MLI layer in the V filter (S) is 4.43. This value can be compared to that of the R filter and I filter; it is expected that the difference in R-V and I-V to be approximately the same, since the spectrum for the spacecraft-facing Kapton MLI in the R and I wavelengths are relatively indistinguishable.

This process is ongoing but shows the methodology of integrating spectral measurements with photometric measurements. The final value obtained from the numerical integration can be compared to other filters and materials to show which materials will have the highest response in each filter without systematic interference or weighted intensities (i.e. CCD is red sensitive).

8. Conclusions

The data presented in this paper shows the first successful steps towards combining laboratory photometric and spectroscopic measurements. The data was compared through B-R curves and proved to be comparable to spectroscopic results. The intensity through the R filter will always be higher if the copper colored Kapton material is showing, and the aluminized backing of the Kapton will have a higher intensity in the B filter. These results showed that the photometric results in B-R are consistent with the spectroscopic data.

The B-R curves also showed that when the MLI targets are rotated over 360 degree rotations, the specular reflections are visible in the Kapton and aluminized backing, when the maximum area of the respective piece faces the CCD. The intensity plots showed that the intact piece had a much smoother curve, than the separate layers of MLI; therefore the contour of the target dramatically affects the intensity plot. Using these results may aid in deciphering whether the high A/m objects are intact pieces of MLI or rather layered pieces that have been detached from the parent body.

Future plans will incorporate more filter comparisons, B-V and B-I to aid in identifying the different materials and comparing the results to the spectrum over the respective wavelengths. The results also only showed the intensity and magnitudes at one phase angle, but the next step is to provide photometric light curves at various phase angles so they can be compared with published remote data.

The total throughput of the system was also processed for a piece of MLI in the V-band to demonstrate the next step in target calibration. Using the integrated numerical value for each material in each filter will allow a more robust calibration and more informed comparison between photometry and spectroscopy.

To investigate orbital debris rotations for numerous materials, a rotation over 360 degrees in one axis proves only one possible scenario. An in-depth study of regular and random rotations about different axes and sampling in 4π steradians is an area of future study.

Unfortunately, high A/m materials are not the only objects that orbit Earth. The vast majority are low A/m objects which have far higher potential for catastrophic impact. A model is under development to differentiate material types - plastics, aluminum, and other metals. Using a representative sample of orbital debris materials and the results from different rotations and phase angles we intend to develop a photometric light curve database incorporating photometric and spectroscopic data.

9. References

1. Johnson, N.L., et. al., "NASA's New Breakup Model of Evolve 4.0", *Advanced Space Res*earch, Vol. 28, No. 9, pp. 1377-1384, 2001.
2. Schildknecht, T. et. Al., "Properties of the High Area-to Mass Ratio Space Debris Population in GEO", 2005 AMOS Technical Conference Proceedings, Kihei, Maui, HI, 2005
3. Payne, T. E., et. al.., "The Development of a Satellite Signatures Testbed Based on the Raven System", 2004 SPIE Astronomical Telescopes and Instrumentation Conference, Glasgow, Scotland, UK, June 2004.
4. Jorgensen, K., *Using Reflectance Spectroscopy to Determine Material Type of Orbital Debris*, Ph.D. Thesis, University of Colorado, Boulder, May 2000.
5. Howell, S., "Handbook of CCD Astronomy", Cambridge University Press, 2000.
6. Rodriguez, Heather, et, al. "Using Light Curves to Characterize Size and Shape of Pseudo-Debris", 2006 AMOS Technical Conference Proceedings, Kihei, Maui, HI, 2006.
7. Carroll, B. and D. Ostlie, *Modern Astrophysics*, Addison-Wesley Publishing Company, INC., 1996.
8. NASA Safety Standard Guidelines and Assessment Procedures for Limiting Orbital Debris, NSS1740.14, August 1995
9. Mulrooney, M. , private communication, 2007.
10. Mulrooney, M., *A 3.0 meter Liquid Mirror Telescope,* Ph.D. Thesis, Rice University, Houston, TX 2000.